

Resonance structures in kink-antikink scattering in a quantum vacuum

Mainak Mukhopadhyay^{✉*}

*Department of Physics; Department of Astronomy and Astrophysics;
Center for Multimessenger Astrophysics, Institute for Gravitation and the Cosmos,
The Pennsylvania State University, University Park, Pennsylvania 16802, USA*

Tanmay Vachaspati^{✉†}

Physics Department, Arizona State University, Tempe, Arizona 85287, USA



(Received 13 March 2023; accepted 31 May 2023; published 22 June 2023)

We investigate kink-antikink scattering in the $\lambda\phi^4$ model in the presence of an additional scalar field, ψ , that is in its quantum vacuum and interacts with ϕ via a $\xi\phi^2\psi^2$ term where ξ is the coupling. The final state of such a scattering is either a bound state with eventual annihilation or a reflection of the kink-antikink pair. Without the ψ field, the outcome is known to depend fractally on the initial velocity of the kink-antikink pair. In the quantum vacuum of the ψ field, the fractal dependence gets modified and disappears above a critical interaction strength, $\xi \approx 0.1$.

DOI: [10.1103/PhysRevD.107.116017](https://doi.org/10.1103/PhysRevD.107.116017)

I. INTRODUCTION

The interactions and scattering of topological defects has been an important area of research with applications to condensed matter systems [1–12] and cosmology [13–16]. Since topological defects are solutions to classical equations of motion, most analyses have considered classical scattering. This has led to important results such as the universality of vortex reconnections [17] and fractal behavior in the scattering of $\lambda\phi^4$ kinks in 1 + 1 dimensions [18–26]. Applications of kink-antikink scattering [27] include the formation of abnormal nuclei [28,29], domain walls in crystals [30,31], folding of protein chains [32,33], and molecular dynamics [34,35].

We are interested in examining how quantum effects modify kink scattering. The inclusion of quantum effects presents some challenges as defects are described as classical objects, while other excitations of interest are quantum in nature. As a result, one has to couple classical and quantum degrees of freedom and to include the quantum backreaction on the classical degrees of freedom. Fortunately much work has been done in this area and now there is a convenient framework called the “classical-quantum correspondence” (CQC) in which certain

quantum systems can be solved in terms of a classical system of equations [36–39]. Quantum backreaction on classical systems is in general difficult to resolve satisfactorily and is also mired in interpretations of quantum mechanics. However, the semiclassical approximation offers a path forward and we utilize it in this work.

There are only two outcomes possible in the scattering of a kink and an antikink in the $\lambda\phi^4$ model: (1) the formation of a bound state (“bion”) and eventual annihilation, and (2) the kink and the antikink reflect and escape to infinity. However, detailed analysis [20,21,25] shows that which of these outcomes occurs depends sensitively on the initial scattering velocity, although at a coarse level, low initial velocity kinks annihilate and high initial velocity kinks reflect. For intermediate velocities, either outcome can result depending on the precise value of the initial velocity: there are windows of low initial velocities for which the kink-antikink reflect off each other instead of annihilating and there is a “fractal” structure in the space of initial velocities.¹ The explanation of this nontrivial dependence involves the resonant energy transfer mechanism among the internal modes (the zero mode and the shape mode) of the kink and antikink. Recent analyses in which the classical field dynamics is truncated to just the kink translation and shape modes shows good agreement with the full field evolution [41,42]. Quantum effects in topologically nontrivial kink backgrounds have received significant attention in the past [43,44] and more recently

*mkm7190@psu.edu

†tvachasp@asu.edu

Published by the American Physical Society under the terms of the Creative Commons Attribution 4.0 International license. Further distribution of this work must maintain attribution to the author(s) and the published article’s title, journal citation, and DOI. Funded by SCOAP³.

¹This is an abuse of the word “fractal” since that generally involves some self-similarity. The structure here is similar to the stability bands in solutions of the Mathieu equation [40].

in [45–47]. Here we are interested in quantum effects in the zero topological charge sector as we have a background of both a kink and an antikink.

The minimal scheme to study quantum effects during kink-antikink scattering is to include quantum fluctuations of the ϕ field of the $\lambda\phi^4$ model itself. In other words, we only have one scalar field ϕ that is decomposed into a classical kink-antikink background (ϕ_c) and quantum excitations on top of this background ($\hat{\phi}$),

$$\phi = \phi_c + \hat{\phi}. \quad (1)$$

A straightforward analysis of this system, however, runs into trouble—we find that $\phi_c \rightarrow 0$ with time. The difficulty can be traced to the use of the semiclassical approximation in a double well potential since the wave functional is not Gaussian and, in fact, may be bimodal. It is possible that some of the problems we encountered may be due to the use of a finite lattice. The full resolution of the difficulties is not clear to us. Hence we study quantum effects of the vacuum of a second scalar field ψ on kink-antikink scattering of the *classical* field ϕ . The main result of our analysis is the change in the fractal structure of the scattering as a function of the interaction strength between ϕ and ψ .

In Sec. II we setup the model and discuss the known results for the classical scattering of kink-antikink in the $\lambda\phi^4$ model. We include the quantum field in Sec. III and we describe the CQC. Finally in Sec. IV we solve the entire system, including backreaction. Our results are summarized in Sec. V. We discuss the main conclusions along with the importance and future prospects related to this work in Sec. VI. We work in natural units, i.e., $\hbar = c = 1$.

II. DYNAMICS OF THE CLASSICAL BACKGROUND

We consider a real classical scalar field ϕ in $1+1$ dimensions in the $\lambda\phi^4$ theory. The Lagrangian density for the system is

$$\mathcal{L}_\phi = \frac{1}{2}\dot{\phi}^2 - \frac{1}{2}\phi'^2 - \frac{\lambda}{4}(\phi^2 - \eta^2)^2, \quad (2)$$

where, λ and η are parameters of the theory. The $\lambda\phi^4$ potential has two minima corresponding to $\phi = \pm\eta$. The Lagrangian density in Eq. (2) is invariant under the transformation, $\phi \rightarrow -\phi$ and hence has a *reflectional* Z_2 symmetry.² The dynamics of the field ϕ has been well-studied in the literature [20,21,43] and is given by the equation of motion,

$$\ddot{\phi} - \phi'' + \lambda(\phi^2 - \eta^2)\phi = 0 \quad (3)$$

By suitable rescalings, the parameters λ and η can be eliminated from the equation of motion, effectively setting $\lambda = 1$ and $\eta = 1$. From the Lagrangian density in Eq. (2) the conserved energy of the classical background configuration (E_ϕ) is given by,

$$E_\phi = \int dx \left[\frac{1}{2}\dot{\phi}^2 + \frac{1}{2}\phi'^2 + \frac{\lambda}{4}(\phi^2 - \eta^2)^2 \right]. \quad (4)$$

The equation of motion admit kink (and antikink) solutions $\phi_{0K(\bar{K})}(t, x)$. One can easily Lorentz boost these solutions to obtain,

$$\phi_{0K(\bar{K})}(t, x) = \pm\eta \tanh \left(\eta \sqrt{\frac{\lambda}{2}} \gamma (x - vt) \right), \quad (5)$$

where, the sign in front corresponds to the kink (antikink) solution which moves in the positive x direction with a constant velocity v and with Lorentz factor $\gamma = 1/\sqrt{1-v^2}$. The total energy of such a configuration is given by,

$$E_{0K(\bar{K})} = \frac{2\sqrt{2}}{3} \gamma \sqrt{\lambda} \eta^3. \quad (6)$$

We are interested in scattering a kink and an antikink. Unlike in the integrable sine-Gordon model, the $\lambda\phi^4$ model does not have a closed form solution in which both a kink and an antikink are present. However, assuming that the kink-antikink start out far enough from each other the interaction energy between them is minimal and we can construct a field configuration of the following form,

$$\phi_{K\bar{K}}(t, x) = \eta \left[\tanh \left(\eta \sqrt{\frac{\lambda}{2}} \gamma (x + \Delta) \right) - \tanh \left(\eta \sqrt{\frac{\lambda}{2}} \gamma (x - \Delta) \right) + 1 \right], \quad (7)$$

where, the kink and the antikink are initially displaced by a distance, $\Delta = v_{\text{in}} t_0$, where t_0 is negative (and is set to -100 in our simulations).³ The kink collision occurs at $t = 0$. The above configuration has a kink and an antikink moving toward each other with an initial velocity v_{in} . When the kink and the antikink get close and start to interact, the above configuration is no longer appropriate. One then needs to solve the equation of motion in Eq. (3), with initial conditions specified by Eq. (7) to get the dynamics of the field ϕ . The kink-antikink pair collides, and either forms a bound state (which is also called a bion) that eventually decays into radiation or are reflected and travel away from

²The kinks (or antikinks) of this model are hence also known as Z_2 kinks (or antikinks).

³The unit of time is $(\sqrt{\lambda}\eta)^{-1}$, and is set to 1.

each other. This outcome depends on the initial velocity v_{in} and the nonintegrability of the $\lambda\phi^4$ model makes it difficult to intuit about this dependence. Hence numerical simulations need to be used, the details of which are discussed in Appendix A.

A. Resonance structures in classical $\lambda\phi^4$ kink-antikink scattering

If a bion does not form, the kink and antikink reflect back with a definite final velocity v_{fin} . If a bion does form and the kink-antikink annihilate, we define $v_{\text{fin}} = 0$. The ratio of the final velocity of the kinks to the initial velocity ($v_{\text{fin}}/v_{\text{in}}$) depends on the initial velocity (v_{in}) and is shown in Fig. 1, a result that has been obtained and discussed extensively in Refs. [20,25]. We present it here using our numerical calculations as a benchmark and most importantly to compare with the evolution when quantum backreaction is included. Similar to prior literature, we notice the fractal structures in the plot, which indicate certain initial velocities for which the kink and the antikink reflect and other windows of initial velocity in which the kinks annihilate. The annihilation windows start out being broad but become thinner as the initial velocity increases. Finally from $v_{\text{in}} \sim 0.26$ the windows cease to form and we have reflection for all $v_{\text{in}} \gtrsim 0.26$. In Ref. [25] the authors extended the initial velocities to $v_{\text{in}} = 0.9$ but did not see any bound state formation post $v_{\text{in}} \sim 0.26$.

This fractal structure has been extensively studied and well understood in the literature. The kinks (or antikinks) in the $\lambda\phi^4$ model have two distinct excitation eigenmodes. One of them corresponds to translations of the kink, known as the zero mode, and the other to the internal vibrations of the kink (or antikink) known as the shape mode [43,44]. In addition, there is a continuum of radiative modes on the kink background.

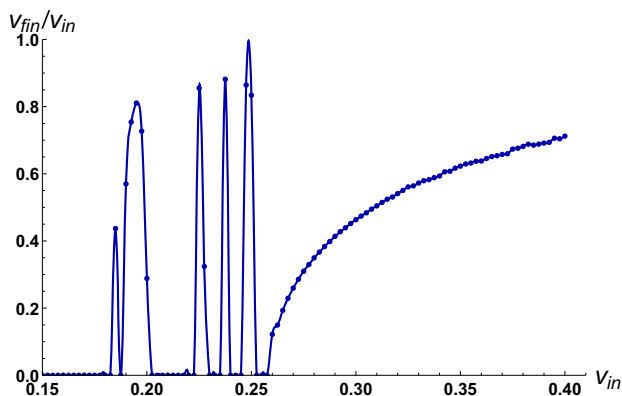


FIG. 1. The ratio of the final velocity to the initial velocity ($v_{\text{fin}}/v_{\text{in}}$) to the initial velocity (v_{in}). Note that $v_{\text{fin}} = 0$ denotes the formation of a bound state. The curves interpolate between the actual data points. The parameters used are $\lambda = 1$, $\eta = 1$, $L = 100$, $N = 500$, and $t_0 = -100$.

When the kink and the antikink collide the kinetic energy is redistributed between these modes and some of it is radiated. In cases, where the kinetic energy is reduced to an extent where the kink-antikink do not have enough energy left, leads to the formation of a bound state, whereas if the decrease is not enough, they separate and reflect off each other. However, in some cases there is a *resonant energy transfer* where the shape mode returns some of the kinetic energy to the zero mode leading the kink and the antikink to separate and not form a bound state. This accounts for the windows we see in Fig. 1. It may be worthwhile to note here given infinite precision, one would find infinite number of subsequent narrower windows for $v_{\text{in}} \lesssim 0.26$ [25].

III. DYNAMICS OF THE QUANTUM FIELD WITHOUT BACKREACTION

We now focus on the dynamics of the quantum field. It is evident that since the quantum field is coupled to the classical background, the nonadiabatic dynamics of the background will lead to particle production of the quantum field. We will use the well-studied ‘classical-quantum correspondence (CQC) [36–39,48,49] technique to address this problem.

The full Lagrangian density for the background ϕ coupled to a quantum field ψ in 1 + 1 dimensions is given by,

$$\mathcal{L} = \mathcal{L}_\phi + \frac{1}{2}(\partial_\mu\psi)^2 - \frac{1}{2}\mu^2\psi^2 - \frac{\xi}{2}\phi^2\psi^2, \quad (8)$$

where, μ is the mass of the quantum field, ξ is the coupling strength, and \mathcal{L}_ϕ is defined in Eq. (2). The truncated Lagrangian density from Eq. (8) for the quantum field ψ can be written as,

$$\mathcal{L}_\psi = \frac{1}{2}\dot{\psi}^2 - \frac{1}{2}\psi'^2 - \frac{1}{2}\mu^2\psi^2 - \frac{\xi}{2}\phi^2\psi^2, \quad (9)$$

where, the time-dependent background $\phi(t, x)$ is given by Eq. (3) if we ignore the backreaction of the quantum field on the classical background. Taking a closer look at the above equation it is evident that the Lagrangian density represents a free scalar field with a space- and time-dependent mass-squared $M^2(t, x)$,

$$M^2(t, x) = \mu^2 + \xi\phi^2(t, x). \quad (10)$$

The faster this term changes the more particle production occurs for the quantum field. Just like for the classical background, we require numerical simulations for having a quantitative understanding of the dynamics of the quantum field. We now turn to doing that.

To begin with, the spatial dimension x is discretized on a *circular* lattice of length L . We consider N evenly spaced

points on the lattice, leading to a lattice spacing of $a = L/N$. The discretized field values are defined as, $\phi_i = \phi(t, -L/2 + ia)$ and $\psi_i = \psi(t, -L/2 + ia)$, where, $i = 1, 2, \dots, N$. The discretized Lagrangian will now be,

$$L_{\psi,\text{disc}} = a \sum_{i=1}^N \left[\frac{1}{2} \dot{\psi}_i^2 + \frac{1}{2} \psi_i \left(\frac{\psi_{i+1} - 2\psi_i + \psi_{i-1}}{a^2} \right) - \frac{1}{2} \mu^2 \psi_i^2 - \frac{\xi}{2} \phi_i^2 \psi_i^2 \right]. \quad (11)$$

Note that we have performed a spatial integration by parts in writing the gradient term above. Let us now switch to a more compact matrix notation, where we can define a column vector for the discretized ψ field as, $\boldsymbol{\psi} = (\psi_1, \psi_2, \dots, \psi_N)^T$. In this notation, the discretized Lagrangian ($L_{\psi,\text{disc}}$) is,

$$L_{\psi,\text{disc}} = \frac{a}{2} \dot{\boldsymbol{\psi}}^T \dot{\boldsymbol{\psi}} - \frac{a}{2} \boldsymbol{\psi}^T \boldsymbol{\Omega}^2 \boldsymbol{\psi}, \quad (12)$$

where $\boldsymbol{\Omega}^2$ is an $N \times N$ matrix defined as,

$$[\boldsymbol{\Omega}^2]_{ij} = \begin{cases} +2/a^2 + M^2(t, x), & i = j \\ -1/a^2, & i = j \pm 1 \pmod{N} \\ 0, & \text{otherwise,} \end{cases} \quad (13)$$

where, $M^2(t, x)$ is defined in Eq. (10) and we now replace ϕ by the discretized value of ϕ at a point i , ϕ_i . The conjugate momentum $\boldsymbol{\pi}$ can be calculated from Eq. (12) which allows us to define the discretized Hamiltonian ($H_{\psi,\text{disc}}$) as,

$$H_{\psi,\text{disc}} = \frac{a}{2} \boldsymbol{\pi}^T \boldsymbol{\pi} + \frac{a}{2} \boldsymbol{\psi}^T \boldsymbol{\Omega}^2 \boldsymbol{\psi}. \quad (14)$$

We now move on to quantizing the theory. This is achieved in the Heisenberg picture by promoting the discretized field value ψ_i to an operator $\hat{\psi}_i$ at the lattice point i . Following [36,37], we introduce the complex time-dependent matrix \mathbf{Z} . The elements of \mathbf{Z} , Z_{ij} satisfy the following relation,

$$\hat{\psi}_i = Z_{ij}^* \hat{a}_j(t_0) + Z_{ij} \hat{a}_j^\dagger(t_0), \quad (15)$$

where, we assume that the background is static for any time $t \leq t_0$. The complete dynamics of $\hat{\psi}_i$ is given by,

$$\ddot{\mathbf{Z}} + \boldsymbol{\Omega}^2 \mathbf{Z} = 0, \quad (16)$$

with the specific initial conditions,

$$\mathbf{Z}(t_0) = -\frac{i}{\sqrt{2a}} \boldsymbol{\Omega}(t_0)^{-1/2}, \quad \dot{\mathbf{Z}}(t_0) = \frac{1}{\sqrt{2a}} \boldsymbol{\Omega}(t_0)^{1/2}. \quad (17)$$

The above initial conditions come with a small caveat. The initial vacuum for the quantum field is chosen around a static background that is given by the initial conditions, but the background is not static and has some time dependence due to the initial velocities of the kinks. This leads to some unwanted but small excitations in the ψ field, which are radiated out even before the kinks have collided. This gives a small error $\lesssim 0.1\%$ of the total energy in the initial conditions for the range of initial velocities v_{in} we have investigated.

IV. DYNAMICS WITH BACKREACTION

We now focus on the main aspect of this work—the dynamics of the classical background coupled to the quantum field including backreaction. In this scenario, the dynamics of the classical background ϕ also gets a contribution from the ψ field,

$$\ddot{\phi} - \phi'' + [\lambda(\phi^2 - \eta^2) + \xi\psi^2]\phi = 0. \quad (18)$$

To take the effects of the quantum field ψ into account we can use the semiclassical approximation in which ψ^2 is replaced by $\langle 0|\hat{\psi}^2|0\rangle \equiv \langle \hat{\psi}^2 \rangle$, where the expectation value is calculated in the vacuum state of the quantum field $\hat{\psi}$. (States do not evolve in the Heisenberg picture.) The background equation can now be written as,

$$\ddot{\phi} - \phi'' + [-m_b^2 + \lambda\phi^2 + \xi\langle \hat{\psi}^2 \rangle]\phi = 0. \quad (19)$$

where $m_b^2 \equiv \lambda\eta^2$. The parameters in (19) should be thought of as bare parameters that will get renormalized due to the quantum field $\hat{\psi}$. We only need to consider “mass renormalization” to the order we are working in and we can write,

$$\ddot{\phi} - \phi'' + [-m^2 + \lambda\phi^2 + \xi(\langle \hat{\psi}^2 \rangle - \langle \hat{\psi}^2 \rangle_{\phi=\eta})]\phi = 0. \quad (20)$$

where the subscript $\phi = \eta$ implies that the expectation value is to be taken in the ground state of $\hat{\psi}$ in the trivial background $\phi = \eta$. Now m^2 is the physical mass parameter and is related to m_b^2 by

$$m^2 = m_b^2 - \xi \langle \hat{\psi}^2 \rangle_{\phi=\eta}. \quad (21)$$

In its discretized form Eq. (20) is,

$$\ddot{\phi}_i - \frac{1}{a^2} (\phi_{i+1} - 2\phi_i + \phi_{i-1}) + \left[-m^2 + \lambda\phi_i^2 + \xi \sum_{j=1}^N (|Z_{ij}|^2 - |Z_{ij}|_{\phi=\eta}^2) \right] \phi_i = 0. \quad (22)$$

where we have used [37],

$$\langle \hat{\psi}_i^2 \rangle = \sum_{j=1}^N |Z_{ij}|^2. \quad (23)$$

Thus, Eq. (22) has to be solved for ϕ_i with initial conditions,

$$\begin{aligned} \phi_i(t_0) &= \phi_{K\bar{K}}(t_0, -L/2 + ia), \\ \dot{\phi}_i(t_0) &= \dot{\phi}_{K\bar{K}}(t_0, -L/2 + ia), \end{aligned} \quad (24)$$

where, as before, $i = 1, 2, \dots, N$ and $\phi_{K\bar{K}}(t, x)$ is given by Eq. (7).

The complete backreacted dynamics is given by Eqs. (22) and (16), with initial conditions given by Eqs. (24) and (17).

A. Energy

The conserved total energy of the system (E) is given by,

$$E = E_\phi + E_\psi^{(R)}, \quad (25)$$

where, E_ϕ is the energy in the classical background and $E_\psi^{(R)}$ is the renormalized energy in the quantum field. The total energy in the classical background can be defined as,

$$\begin{aligned} E_\phi &= a \sum_{i=1}^N \rho_{\phi,i} = a \sum_{i=1}^N \left[\frac{1}{2} \dot{\phi}_i^2 + \frac{1}{4a^2} ((\phi_{i+1} - \phi_i)^2) \right. \\ &\quad \left. + (\phi_i - \phi_{i-1})^2 + \frac{\lambda}{4} (\phi_i^2 - \eta^2)^2 \right]. \end{aligned} \quad (26)$$

The energy in the quantum field is,

$$E_\psi \equiv \langle 0 | \hat{H}_{\psi, \text{disc}} | 0 \rangle = \frac{a}{2} \text{Tr} \left(\dot{\mathbf{Z}}^\dagger \dot{\mathbf{Z}} + \mathbf{Z}^\dagger \Omega^2 \mathbf{Z} \right). \quad (27)$$

The discretized energy density in $\hat{\psi}$ can be defined as,

$$\begin{aligned} \rho_{\psi,i} &= \sum_{j=1}^N \left[\frac{1}{2} |\dot{Z}_{ij}|^2 + \frac{1}{4a^2} \left\{ |Z_{i+1,j} - Z_{ij}|^2 \right. \right. \\ &\quad \left. \left. + |Z_{ij} - Z_{i-1,j}|^2 \right\} + \frac{1}{2} \left\{ \mu^2 + \xi \phi_i^2 \right\} |Z_{ij}|^2 \right]. \end{aligned} \quad (28)$$

Similar to the renormalized mass defined in (21), the renormalized energy density in the quantum field may be defined as,

$$\rho_{\psi,i}^{(R)} = \rho_{\psi,i} - \rho_{\psi,i}|_{\phi=\eta}, \quad (29)$$

where, we subtract the energy density of the quantum field in the trivial vacuum ($\phi = \eta$) from the energy density. Hence, the renormalized total energy in the quantum field is,

$$E_\psi^{(R)} = E_\psi - E_\psi|_{\phi=\eta}. \quad (30)$$

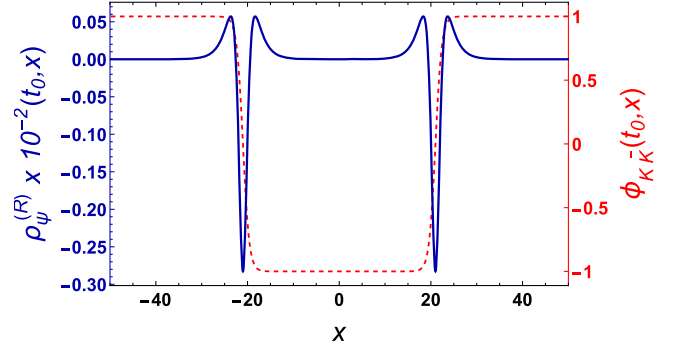


FIG. 2. The initial renormalized energy density in ψ (solid dark blue curve) and the initial profile of the kink-antikink background ϕ (dashed red curve). We note that the kink and the antikink is dressed with the ψ particles. The main parameters are: $v_{\text{in}} = 0.21$, $\xi = 0.05$, $\mu = 0.1$, $\lambda = 1$, $\eta = 1$, $L = 100$, $N = 500$, and $t_0 = -100$.

B. Initial structure of the vacuum

The initial vacuum structure of the quantum field can be visualized from Fig. 2. In the figure, we show the initial renormalized energy density of ψ , $[\rho_{\psi,i}^{(R)}(t = t_0, x)]$. The figure also shows the background ϕ at the initial time $\phi_{K\bar{K}}(t = t_0, x)$ [see Eq. (24)]. In the trivial vacuum, $\phi = \eta$, the renormalized energy density in ψ vanishes, as in Fig. 2 at the boundaries of the lattice. However, at the position of the kink and the antikink, there is a big dip in the energy density of ψ that depends on the parameters of the model. The dips are the ground state of ψ in this particular (kink-antikink) background. As the background changes, that is, as the kink-antikink move, the dips move along with them. This will be evident in Sec. VA where we study dynamics of the background.

V. RESULTS

Our numerical methods and checks are described in Appendix A and B.

A. Quantum kink-antikink scattering with backreaction

In Fig. 3 we show the energy density in the background field ϕ —the expression in rectangular brackets in Eq. (26)—as a function of time (vertical axis). The top panels compare the classical evolution ($\xi = 0$) for $v_{\text{in}} = 0.21$, when a bion forms, and for $v_{\text{in}} = 0.30$, when the kinks reflect. The bottom two panels show the corresponding evolution for ($\xi = 0.05$). The bion is now tighter; the reflected kinks have smaller velocity. The behavior is expected since the kinks in the $\xi \neq 0$ case excite the quantum vacuum of $\hat{\psi}$, produce particles, and lose energy during the evolution. The energy in $\hat{\psi}$ must come from the kinetic energy of the kinks which results in a tighter bion for $v_{\text{in}} = 0.21$ and for slower reflected kinks for $v_{\text{in}} = 0.30$. In the case $v_{\text{in}} = 0.21$, where the final state is a bound state,

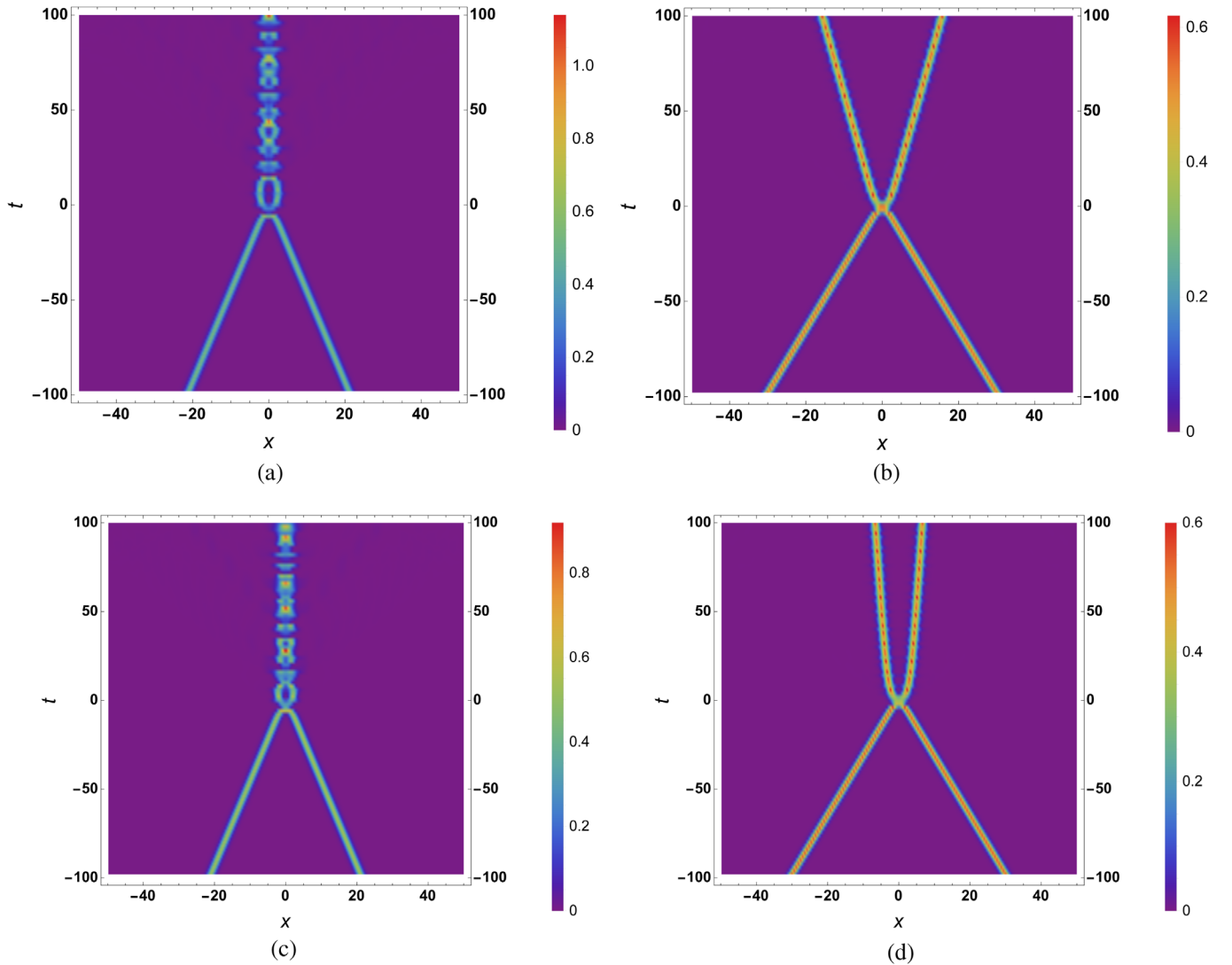


FIG. 3. Density plots showing the time evolution of the energy density ($\rho_{\phi,i}$) in the background [see Eq. (26)]. Top panel: classical evolution—(a) $v_{\text{in}} = 0.21$ where the final state is a bound state, (b) $v_{\text{in}} = 0.3$ to show a case where the kink and the antikink get reflected postcollision. Bottom panel: evolution including coupling to the quantum field and backreaction—(c) same as (a), (d) same as (b). The parameters are: $\xi = 0.05$, $\mu = 0.1$, $\lambda = 1$, $\eta = 1$, $L = 100$, $N = 500$, and $t_0 = -100$ for all the cases. The animations corresponding to the different cases can be found at [50].

we see that the kink and the antikink travel toward each other, collide and get stuck leading to a caterpillar-like structure in Fig. 3. Each segment of the caterpillar shows that the kinks separate for a short duration but then come back and collide again. This repeats for some time and finally the kink-antikink do not have enough energy to separate and hence lose their individual identity to form a bound state (or bion) that decays into radiation. It is difficult to see the difference between Figs. 3a and 3c, since in both cases the caterpillar structure exists and repeated collisions makes it difficult to notice any differences. To clarify the differences, we plot the value of the background ϕ at the center of the lattice, $\phi(t, x = 0)$, in Fig. 4 for $v_{\text{in}} = 0.21$ and for $v_{\text{in}} = 0.30$. In Fig. 5 we show the time dependence of the energy in the ϕ

background [see Eq. (26)]. Before the collision, the energy in the background is constant and is given by twice that of the single kink (or antikink) energy [see Eq. (6)], which is basically the sum of the individual energies of the kink and the antikink. For the classical evolution (dashed curves), E_ϕ is the total energy and is conserved. In the presence of the quantum field, the outcome depends on v_{in} . When a bound state is formed (solid dark blue curve), the repeated collisions lead to a cascading drop in E_ϕ and the lost energy goes into radiating ψ particles.

The loss of energy from the kinks to ψ quanta can be visualized in Fig. 6. The plot shows the time evolution of the renormalized energy density in ψ , denoted by $\rho_\psi^{(R)}$ [see Eqs. (28), (29)]. As we have noted in Fig. 2, there is a

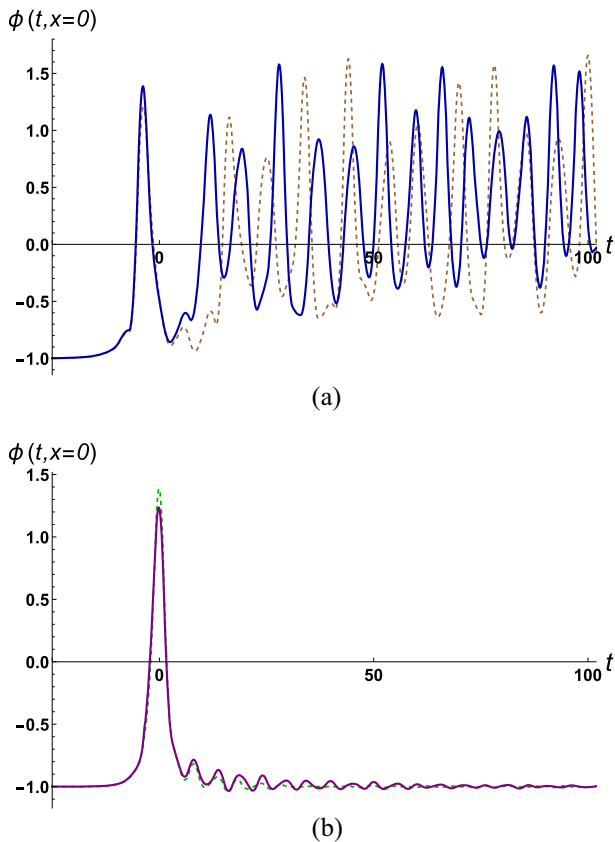


FIG. 4. Time evolution of the value of the background ϕ at the center of the lattice $\phi(t, x = 0)$ contrasting the classical evolution (dashed) with the case including quantum backreaction (solid) for (a) $v_{\text{in}} = 0.21$ (brown and dark blue respectively) and (b) $v_{\text{in}} = 0.3$ (dark green and purple respectively). The parameters used are the same as the ones stated in Fig. 3.

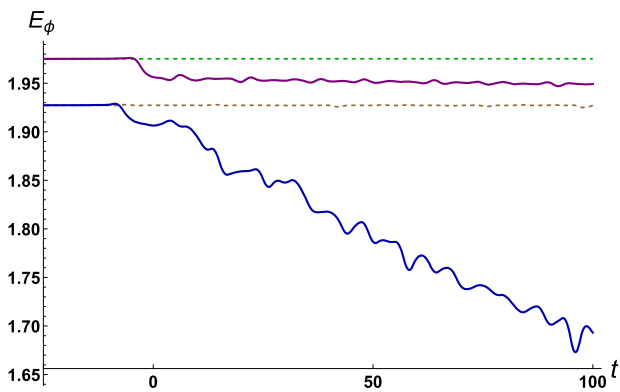


FIG. 5. Time evolution of the total energy in the background ϕ (E_ϕ) for the classical evolution (dashed) and the case including quantum backreaction (solid) for—(a) $v_{\text{in}} = 0.21$ (brown and dark blue respectively) and (b) $v_{\text{in}} = 0.3$ (dark green and purple respectively). The parameters used are the same as the ones stated in Fig. 3.

“cloud” of ψ around the position of the kink. This cloud perfectly follows the kink and the antikink at early times as can be seen by comparing Figs. 3 and 6.

The collisions are visible as the segments of the caterpillar after $t = 0$. In the $v_{\text{in}} = 0.21$ case, as the kinks collide, separate and collide again, we see bursts of radiation that are produced, which then propagate outward away from the center. By virtue of periodic boundary conditions, once the radiation reaches the end of the lattice they wrap around and return back toward the center. The bursts of radiation in the case of a bound state formation is what is observed in Fig. 5 (solid dark blue curve), as a cascading decrease in the total energy in the background.

When the kink-antikink pair is reflected, as in Fig. 6(b), there is a burst of ψ radiation at the time of collision seen as the two yellow bands moving out from the collision point in the figure. After the collision, the ψ clouds keep moving with the kink and the antikink but the kink internal modes are excited and there are some weaker bursts of ψ radiation. There are the light yellow bands being radiated out as the kinks move away from each other in Fig. 6(b). The energy loss appears as the undulating features in the $v_{\text{in}} = 0.30$ curve at late times in Fig. 5. Finally we come to our main objective of examining how the fractal nature of the classical scattering shown in Fig. 1 changes when the kinks scatter in the quantum vacuum of a second field. The results are presented in Fig. 7. The dashed gray curve shows the results of the classical scattering and is the same as presented in Fig. 1. The other curves show the results of the scattering as we turn up the interaction strength ξ . An increase in ξ shifts the scattering peaks to higher v_{in} but also reduces the peak $v_{\text{fin}}/v_{\text{in}}$. The critical v_{in} above which there is no further fractal structure also increases with increasing ξ . For example, for $\xi = 0$ the critical v_{in} is ~ 0.26 while for $\xi = 0.1$ it is ~ 0.37 . Some of these features can be qualitatively understood based on our earlier discussion that the time-dependent background of the scattering kinks excites ψ radiation and causes the kinks to lose kinetic energy. This process makes it easier for the kink-antikink to form a bound state and annihilate and it takes higher initial velocities for the kinks to reflect. Also, in cases that the kinks do reflect, the lost energy means that the final velocities of the kinks will be lower.

We have checked that our results are insensitive to the choice of lattice spacing, a , and to the size of the simulation box, L . A comparison of our results for different choices of a and L is shown in Appendix B.

VI. CONCLUSIONS AND DISCUSSION

While kink-antikink scattering has been thoroughly investigated in the literature [20,21,25], our focus in this work has been on *quantum* effects on the scattering. Even if the kink-antikink propagate in a quantum vacuum, they provide a time-dependent background that can produce

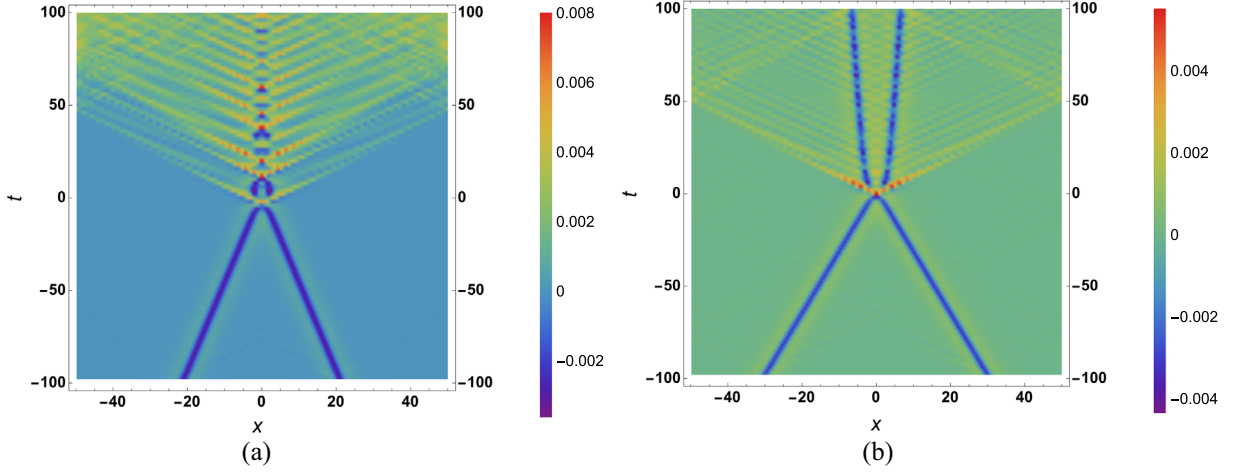


FIG. 6. Time evolution of the renormalized energy density $\rho_\psi^{(R)}$. (a) $v_{\text{in}} = 0.21$ where a bound state is formed and (b) $v_{\text{in}} = 0.3$ where the kink and the antikink undergo reflection. The parameters are the same as for Fig. 3. The animations corresponding to the different cases can be found at [50].

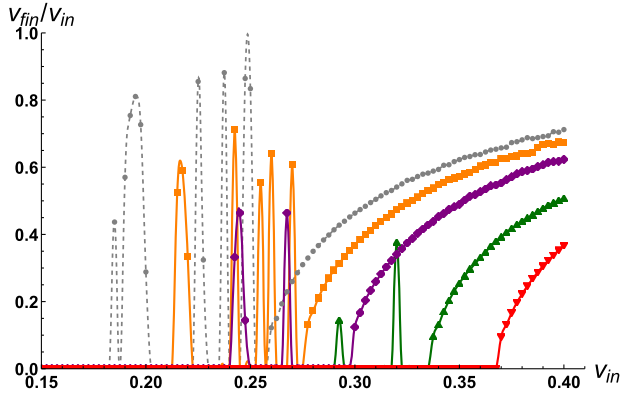


FIG. 7. The ratio of the final velocity to the initial velocity ($v_{\text{fin}}/v_{\text{in}}$) post-collision to the initial velocity (v_{in}). Note that $v_{\text{fin}} = 0$ denotes the formation of a bound state. The dashed gray line shows the classical evolution ($\xi = 0$), whereas the solid lines denote the evolution including quantum backreaction for different values of ξ : $\xi = 0.03$ (orange), $\xi = 0.05$ (purple), $\xi = 0.08$ (dark green), and $\xi = 0.1$ (red). The actual data points are also shown. The other parameters used are: $\mu = 0.1$, $\lambda = 1$, $\eta = 1$, $L = 100$, $N = 500$, and $t_0 = -100$.

particles and radiation, which in turn depletes the kinetic energy of the kinks and modifies the scattering outcomes. The main tool for our analysis was the CQC formalism that enabled us to conveniently use classical equations of motion for the quantum fields. We treated quantum backreaction on the classical background by employing the semiclassical approximation. The main result of this work is summarized in Fig. 7 where we see changes in the fractal structure of the scattering as the interaction strength (ξ) between the kinks and the quantum field increases. For $\xi \gtrsim 0.1$, the fractal structure disappears and there is simply annihilation for $v_{\text{in}} \lesssim 0.37$ and reflection for $v_{\text{in}} \gtrsim 0.37$.

In future we hope to return to examining the effect of quantum fluctuations of the background scalar field itself on the scattering outcome, as mentioned in the Introduction [see Eq. (1)]. To obtain a correspondence between our two field case with ϕ and ψ and the single field case in (1), we can add the equations of motion for ϕ and ψ and compare to the equation of motion obtained using (1). The two equations agree for the special choice of parameters $\mu^2 = -\lambda\eta^2$ and $\xi = 3\lambda$. Our technique fails for these values because then the ψ field has a zero mode (corresponding to the translation mode of the kink). It still might be possible to consider the two field case in the limit that $\mu^2 \rightarrow -\lambda\eta^2$ and $\xi \rightarrow 3\lambda$ and obtain a reasonable approximation to the single field case. Alternatively, perhaps recent progress in dealing with systems containing classical and quantum components will be helpful [51–53].

ACKNOWLEDGMENTS

We thank Omer Faruk Albayrak, Fabio van Dissel, and George Zahariade for useful discussions and Evangelos I. Sfakianakis for comments. M.M. is supported by NSF Grant No. AST-2108466. M.M. also acknowledges support from the Institute for Gravitation and the Cosmos (IGC) Postdoctoral Fellowship. M.M. wishes to thank the Yukawa Institute for Theoretical Physics (YITP), Kyoto University for hospitality where a major part of this work was done. T.V. is supported by the U.S. Department of Energy, Office of High Energy Physics, under Award No. DE-SC0019470.

APPENDIX A: NUMERICAL METHODS

We use the *Verlet* method to solve the coupled differential equations for this work. In particular, we use the position Verlet method as follows,

$$\begin{aligned}
 x_{n+1/2} &= x_n + \frac{1}{2} dt \dot{x}_n, \\
 \dot{x}_{n+1} &= \dot{x}_n + dt \ddot{x}(x_{n+1/2}), \\
 x_{n+1} &= x_{n+1/2} + \frac{1}{2} dt \dot{x}_{n+1}.
 \end{aligned}
 \tag{A1}$$

Although fairly simple, this method is efficient, fast, and gives us accurate results for the current problem. More advanced numerical techniques may be used but given the $\mathcal{O}(N^2)$ complexity of the problem, the requirements of fine spatial and temporal resolution to capture the details of the dynamics, and the necessity to evolve the system for long durations, the current numerical scheme is ideal. We have also verified our benchmark results using a more advanced numerical technique—the explicit Crank-Nicholson method with two iterations, and found no significant difference in the evolution and observable quantities. All the results presented are simulated on a circular lattice of physical length $L = 100$ which is sampled using $N = 500$ points. This implies a spatial resolution $a = L/N = 0.2$. We use a temporal spacing proportional to a , $dt = a/5$. A smaller a would indeed improve the resolution and help us to capture the dynamics even better, but with the current lattice spacing we have a total energy nonconservation due to numerical errors, over the *entire duration of time evolution* of the order of 0.2%. We have also checked that our results are fairly independent of the UV ($a = L/N$) and IR (L) cutoffs. We start the evolution at the initial time, $t_0 = -100$. The collisions happen around $t \sim 0$. The periodic boundary conditions make it necessary to ensure that the finite lattice size does not significantly interfere with our results. Owing to our use of periodic boundary conditions, the radiation propagating outward from the center eventually comes back. Hence, we

only evolve the dynamics for one light crossing time, $t = L = 100$, such that our results are not affected by radiation that re-enters the collision region.

For all the results from here on we assume, $\lambda = 1$ and $\eta = 1$. We choose $\mu = 0.1m$. This is in the regime where $\mu < m$, which is required since m is the mass of the classical background which we expect to be larger than the mass of the quantum field. The two main parameters that we vary are the initial velocity, v_{in} , and the interaction strength, ξ . The initial incoming velocity of the kink-antikink configuration v_{in} is varied between 0.15 and 0.4. We do not consider lower velocities since for such low velocities the final state is fixed to be a bound state and no resonance structures are present, and in this work we are interested in studying quantum modifications to the resonance structures. We do not consider $v_{\text{in}} > 0.4$ since kinks with high initial velocities get reflected. We vary ξ in the range $[0, 0.1]$.

APPENDIX B: ANALYSIS OF THE QUALITY OF NUMERICS

The choice of time-step (dt) should not affect our results in any considerable way. This is shown in Fig. 8. The energy in the background does not show any difference on using a smaller time step ($dt = a/10$, dashed red curve) than what is used for this work ($dt = a/5$, solid blue curve). The total energy nonconservation for the time step we use ($dt = a/5$, solid purple curve) is of the order of $\sim 0.2\%$ over the *entire* time of evolution. This is more than sufficient for the current work. The accuracy of energy conservation increases even more if we take a smaller dt ($= a/10$, solid orange curve), which is to be expected.

One of the main physical observables we are interested in is the energy (E_ϕ) in the background field ϕ and the total

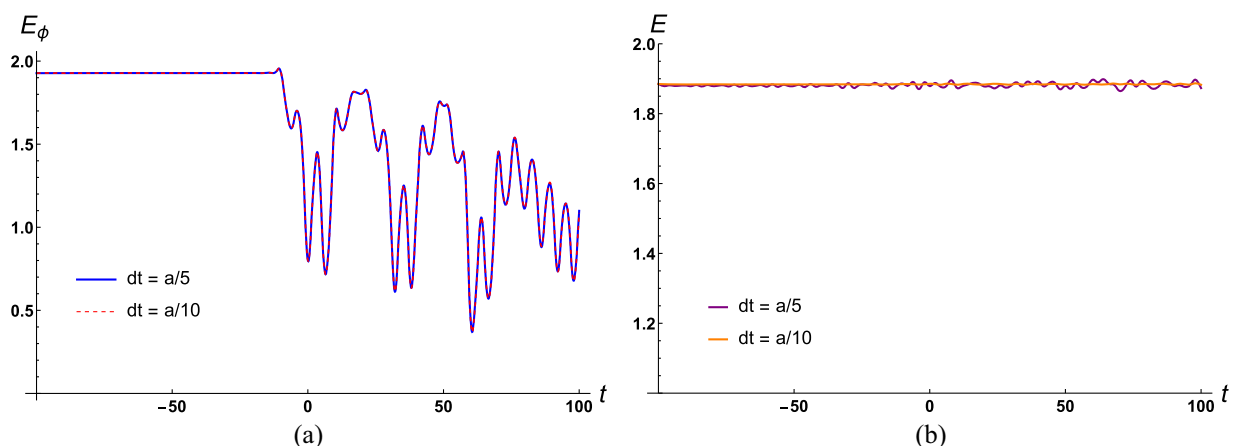


FIG. 8. (a) Time-evolution of the background energy (E_ϕ) for different values of dt . The two curves overlap and are not distinctly visible. (b) Time-evolution of the renormalized total energy E for different values of dt . The plots illustrate the independence of our results to the choice of time step. The other parameters considered are: $v_{\text{in}} = 0.21$, $\xi = 0.5$, $\mu = 0.1$, $\lambda = 1$, $\eta = 1$, $t_0 = -100$, $L = 100$, and $N = 500$. The collision happens at $t = 0$.

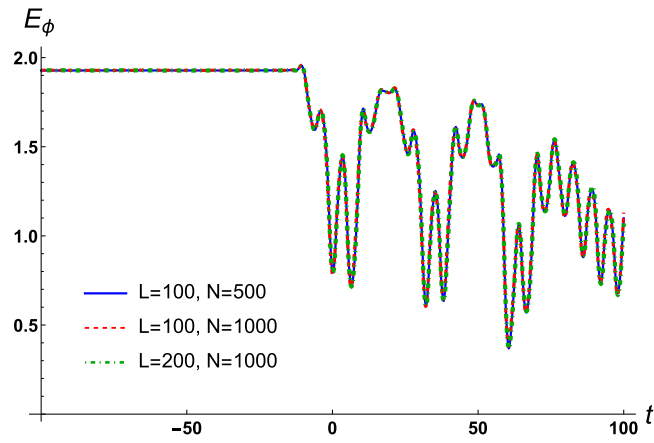


FIG. 9. Time-evolution of the background energy (E_ϕ) for different values of L and N to illustrate the UV- and IR-dependence of our results. The other parameters considered are: $v_{\text{in}} = 0.21$, $\xi = 0.5$, $\mu = 0.1$, $\lambda = 1$, $\eta = 1$, and $t_0 = -100$. The collision happens at $t = 0$. Note, lattice spacing $a = L/N$ and $dt = a/5$.

energy (E) (as discussed in Sec. IV A). As one might expect, these observables should not depend on the discretization scales—the spacing of the lattice (a) and the physical size of the lattice (L). In Fig. 9 we show such is the case, where decreasing the lattice spacing or increasing the physical size of the box has no effect on E_ϕ .

-
- [1] W. Zurek, Cosmological experiments in superfluid helium?, *Nature (London)* **317**, 505 (1985).
- [2] V. Pal, C. Tradonsky, R. Chriki, A. A. Friesem, and N. Davidson, Observing Dissipative Topological Defects with Coupled Lasers, *Phys. Rev. Lett.* **119**, 013902 (2017).
- [3] A. del Campo, G. De Chiara, G. Morigi, M. B. Plenio, and A. Retzker, Structural Defects in Ion Chains by Quenching the External Potential: The Inhomogeneous Kibble-Zurek Mechanism, *Phys. Rev. Lett.* **105**, 075701 (2010).
- [4] I. Chuang, B. Yurke, R. Durrer, and N. Turok, Cosmology in the laboratory: Defect dynamics in liquid crystals, *Science* **251**, 1336 (1991).
- [5] M. J. Bowick, L. Chandar, E. A. Schiff, and A. M. Srivastava, The cosmological Kibble mechanism in the laboratory: String formation in liquid crystals, *Science* **263**, 943 (1994).
- [6] P. C. Hendry, N. S. Lawson, R. A. M. Lee, P. V. E. McClintock, and C. D. H. Williams, Generation of defects in superfluid 4He as an analogue of the formation of cosmic strings, *Nature (London)* **368**, 315 (1994).
- [7] V. M. H. Ruutu, V. B. Eltsov, A. J. Gill, T. W. B. Kibble, M. Krusius, Y. G. Makhlin, B. Plaçaïs, G. E. Volovik, and W. Xu, Vortex formation in neutron-irradiated superfluid 3He as an analogue of cosmological defect formation, *Nature (London)* **382**, 334 (1996).
- [8] C. Bäuerle, Y. M. Bunkov, S. N. Fisher, H. Godfrin, and G. R. Pickett, Laboratory simulation of cosmic string formation in the early universe using superfluid 3He, *Nature (London)* **382**, 332 (1996).
- [9] R. Monaco, J. Mygind, and R. J. Rivers, Zurek-Kibble Domain Structures: The Dynamics of Spontaneous Vortex Formation in Annular Josephson Tunnel Junctions, *Phys. Rev. Lett.* **89**, 080603 (2002).
- [10] R. Carmi, E. Polturak, and G. Koren, Observation of Spontaneous Flux Generation in a Multi-Josephson-Junction Loop, *Phys. Rev. Lett.* **84**, 4966 (2000).
- [11] A. Maniv, E. Polturak, and G. Koren, Observation of Magnetic Flux Generated Spontaneously during a Rapid Quench of Superconducting Films, *Phys. Rev. Lett.* **91**, 197001 (2003).
- [12] J. Beugnon and N. Navon, Exploring the Kibble-Zurek mechanism with homogeneous Bose gases, *J. Phys. B* **50**, 022002 (2017).
- [13] W. H. Zurek, Cosmological experiments in condensed matter systems, *Phys. Rep.* **276**, 177 (1996).
- [14] T. Vachaspati, Topological defects in the cosmos and lab, *Contemp. Phys.* **39**, 225 (1998).
- [15] T. W. B. Kibble, Testing cosmological defect formation in the laboratory, *Physica (Amsterdam)* **369C**, 87 (2002).
- [16] P. A. R. Ade *et al.* (Planck Collaboration), Planck 2013 results. XXV. Searches for cosmic strings and other topological defects, *Astron. Astrophys.* **571**, A25 (2014).
- [17] A. Vilenkin and E. P. S. Shellard, *Cosmic Strings and Other Topological Defects* (Cambridge University Press, Cambridge, England, 2000).
- [18] A. Kudryavtsev, Solitonlike solutions for a Higgs scalar field, Technical Report, Institute of Theoretical and Experimental Physics, 1975.
- [19] T. Sugiyama, Kink-antikink collisions in the two-dimensional ϕ^4 model, *Prog. Theor. Phys.* **61**, 1550 (1979).

- [20] D. K. Campbell, J. F. Schonfeld, and C. A. Wingate, Resonance structure in kink-antikink interactions in ϕ^4 theory, *Physica (Amsterdam)* **9D**, 1 (1983).
- [21] P. Anninos, S. Oliveira, and R. A. Matzner, Fractal structure in the scalar $\lambda(\phi^2 - 1)^2$ theory, *Phys. Rev. D* **44**, 1147 (1991).
- [22] Z. Fei, Y. S. Kivshar, and L. Vázquez, Resonant kink-impurity interactions in the ϕ^4 model, *Phys. Rev. A* **46**, 5214 (1992).
- [23] R. H. Goodman and R. Haberman, Kink-antikink collisions in the ϕ^4 equation: The n-bounce resonance and the separatrix map, *SIAM J. Appl. Dyn. Syst.* **4**, 1195 (2005).
- [24] A. M. Marjaneh, D. Saadatmand, K. Zhou, S. V. Dmitriev, and M. E. Zomorrodian, High energy density in the collision of N kinks in the ϕ^4 model, *Commun. Nonlinear Sci. Numer. Simul.* **49**, 30 (2017).
- [25] A. Alonso Izquierdo, J. Queiroga-Nunes, and L. M. Nieto, Scattering between wobbling kinks, *Phys. Rev. D* **103**, 045003 (2021).
- [26] C. Adam, K. Oles, T. Romanczukiewicz, and A. Wereszczynski, Kink-antikink collisions in a weakly interacting ϕ^4 model, *Phys. Rev. E* **102**, 062214 (2020).
- [27] M. Lizunova and J. van Wezel, An introduction to kinks in ϕ^4 -theory, *SciPost Phys. Lect. Notes* **23**, 1 (2021).
- [28] T. D. Lee and G. C. Wick, Vacuum stability and vacuum excitation in a spin 0 field theory, *Phys. Rev. D* **9**, 2291 (1974).
- [29] J. Boguta, Abnormal nuclei, *Phys. Lett.* **128B**, 19 (1983).
- [30] Y. Wada and J. R. Schrieffer, Brownian motion of a domain wall and the diffusion constants, *Phys. Rev. B* **18**, 3897 (1978).
- [31] R. D. Yamaletdinov, V. A. Slipko, and Y. V. Pershin, Kinks and antikinks of buckled graphene: A testing ground for the ϕ^4 field model, *Phys. Rev. B* **96**, 094306 (2017).
- [32] S. Hu, M. Lundgren, and A. J. Niemi, Discrete frenet frame, inflection point solitons, and curve visualization with applications to folded proteins, *Phys. Rev. E* **83**, 061908 (2011).
- [33] S. Hu, A. Krokhotin, A. J. Niemi, and X. Peng, Towards quantitative classification of folded proteins in terms of elementary functions, *Phys. Rev. E* **83**, 041907 (2011).
- [34] A. Bishop, Defect states in polyacetylene and polydiacetylene, *Solid State Commun.* **33**, 955 (1980).
- [35] M. Rice and E. Mele, Phenomenological theory of soliton formation in lightly-doped polyacetylene, *Solid State Commun.* **35**, 487 (1980).
- [36] T. Vachaspati and G. Zahariade, Classical-quantum correspondence and backreaction, *Phys. Rev. D* **98**, 065002 (2018).
- [37] T. Vachaspati and G. Zahariade, Classical-quantum correspondence for fields, *J. Cosmol. Astropart. Phys.* **09** (2019) 015.
- [38] T. Vachaspati and G. Zahariade, Classical-quantum correspondence and Hawking radiation, *J. Cosmol. Astropart. Phys.* **04** (2019) 013.
- [39] M. Mukhopadhyay and T. Vachaspati, Rolling classical scalar field in a linear potential coupled to a quantum field, *Phys. Rev. D* **100**, 096018 (2019).
- [40] P. Morse and H. Feshbach, *Methods of Theoretical Physics, International Series in Pure and Applied Physics* (McGraw-Hill, New York, 1953).
- [41] N. S. Manton, K. Oles, T. Romanczukiewicz, and A. Wereszczynski, Collective Coordinate Model of Kink-Antikink Collisions in ϕ^4 Theory, *Phys. Rev. Lett.* **127**, 071601 (2021).
- [42] C. Adam, N. S. Manton, K. Oles, T. Romanczukiewicz, and A. Wereszczynski, Relativistic moduli space for kink collisions, *Phys. Rev. D* **105**, 065012 (2022).
- [43] T. Vachaspati, *Kinks and Domain Walls: An Introduction to Classical and Quantum Solitons* (Cambridge University Press, Cambridge, England, 2010).
- [44] R. Rajaraman, *Solitons and Instantons: An Introduction to Solitons and Instantons in Quantum Field Theory, North-Holland Personal Library* (North-Holland Publishing Company, Amsterdam, 1982).
- [45] J. Evslin, Manifestly finite derivation of the quantum kink mass, *J. High Energy Phys.* **11** (2019) 161.
- [46] J. Evslin and A. García Martín-Caro, Spontaneous emission from excited quantum kinks, *J. High Energy Phys.* **12** (2022) 111.
- [47] H. Liu, J. Evslin, and B. Zhang, Meson production from kink-meson scattering, *Phys. Rev. D* **107**, 025012 (2023).
- [48] J. Ollé, O. Pujolas, T. Vachaspati, and G. Zahariade, Quantum evaporation of classical breathers, *Phys. Rev. D* **100**, 045011 (2019).
- [49] M. Mukhopadhyay, E. I. Sfakianakis, T. Vachaspati, and G. Zahariade, Kink-antikink scattering in a quantum vacuum, *J. High Energy Phys.* **04** (2022) 118.
- [50] <https://sites.google.com/asu.edu/mainakm>.
- [51] M. Bojowald and D. Ding, Canonical description of cosmological backreaction, *J. Cosmol. Astropart. Phys.* **03** (2021) 083.
- [52] J. Oppenheim and Z. Weller-Davies, Path integrals for classical-quantum dynamics, [arXiv:2301.04677](https://arxiv.org/abs/2301.04677).
- [53] J. Oppenheim and Z. Weller-Davies, Covariant path integrals for quantum fields back-reacting on classical space-time, [arXiv:2302.07283](https://arxiv.org/abs/2302.07283).